Empowering Adsorption and Photocatalytic Degradation of Ciprofloxacin on BiOI Composites: A Material-by-Design Investigation

Sepideh G. Khasevani, Dariush Nikjoo, Cécile Chaxel, Kentaro Umeki, Shokat Sarmad, Jyri-Pekka Mikkola, and Isabella Concina*

Cite This: ACS Omega 2023, 8, 44044−44056

Read Online

ACCESS | Metrics & More | Article Recommendations | Supporting Information

ABSTRACT: Binary and ternary composites of BiOI with NH_2-MIL-101(Fe) and a functionalized biochar were synthesized through an *in situ* approach, aimed at spurring the activity of the semiconductor as a photocatalyst for the removal of ciprofloxacin (CIP) from water. Experimental outcomes showed a drastic enhancement of the adsorption and the equilibrium (which increased from 39.31 mg g^{-1} of bare BiOI to 76.39 mg g^{-1} of the best ternary composite in 2 h time), while the kinetics of the process was not significantly changed. The photocatalytic performance was also significantly enhanced, and the complete removal of 10 ppm of CIP in 3 h reaction time was recorded under simulated solar light irradiation for the best catalyst of the investigated batch. Catalytic reactions supported by different materials obeyed different reaction

CIPROFLOXACIN REMOVAL

orders, indicating the existence of different mechanisms. The use of scavengers for superoxide anion radicals, holes, and hydroxyl radicals showed that although all these species are involved in CIP photodegradation, the latter play the most crucial role, as also confirmed by carrying out the reaction at increasing pH conditions. A clear correlation between the reduction of BiOI crystallite sizes in the composites, as compared to the bare material, and the material performance as both adsorbers and photocatalyst was identified.
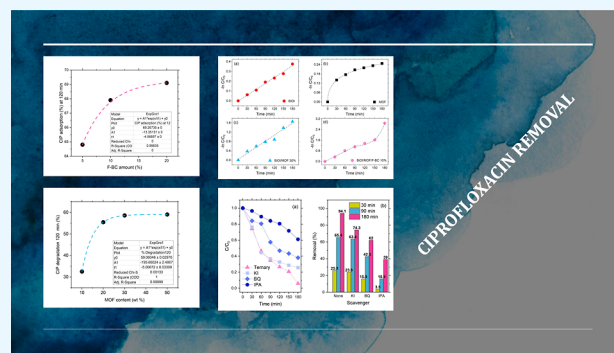
INTRODUCTION

The unwanted release of antibiotic residuals in waters has over time caused the insurgence of antimicrobial resistance, fighting which has been recognized as a priority for global public health. In 2015, WHO issued a global action plan on antimicrobial resistance and urged each country to formulate its own plan.[1] This problem has become even more acute due to the COVID-19 pandemic: according to a recent evaluation, 75% of patients affected by Sars-CoV-2 were given antibiotics,[2] and the extent of the associated water pollution is still hard to estimate. The capability to clean water systems has since then become even more urgent than it used to be.

Different technologies are proposed to face this huge challenge using both physical (isolation and removal of the pollutants) and chemical strategies (transformation of the pollutants into less harmful substances).[3] However, no single approach is capable of facing the water pollution issue as a whole, and a multitechnique strategy should be considered.

Within this framework, engineering efficient, durable, robust, and easy-to-recover adsorbents and photocatalysts can play an important role in contributing to water remediation by either the adsorption of the organic target pollutant or its conversion to less harmful compounds (or in the best case its complete

oxidation to CO_2 and water) or by a combination of these two processes.

Among the bismuth oxyhalides, BiOI is attracting particular attention as a photocatalyst, thanks to its layered structure,[4,5] which is supposedly efficient in transferring photogenerated electron−hole pairs, thus promoting the redox reactions subsequently responsible for the degradation of the target pollutants. Furthermore, the small band gap (around 1.8 eV) of BiOI renders it suitable for visible light absorption.
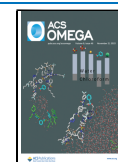
Metal−organic frameworks (MOFs) have recently emerged as potent candidates for photocatalytic water remediation, thanks to their porous structure, high specific surface area, and modifiable structure and properties.[6−9] Among them, iron-based MOFs showed excellent results in Fenton catalysis due to the easy charge exchange in the Fe^{II}/Fe^{III} couple, which,
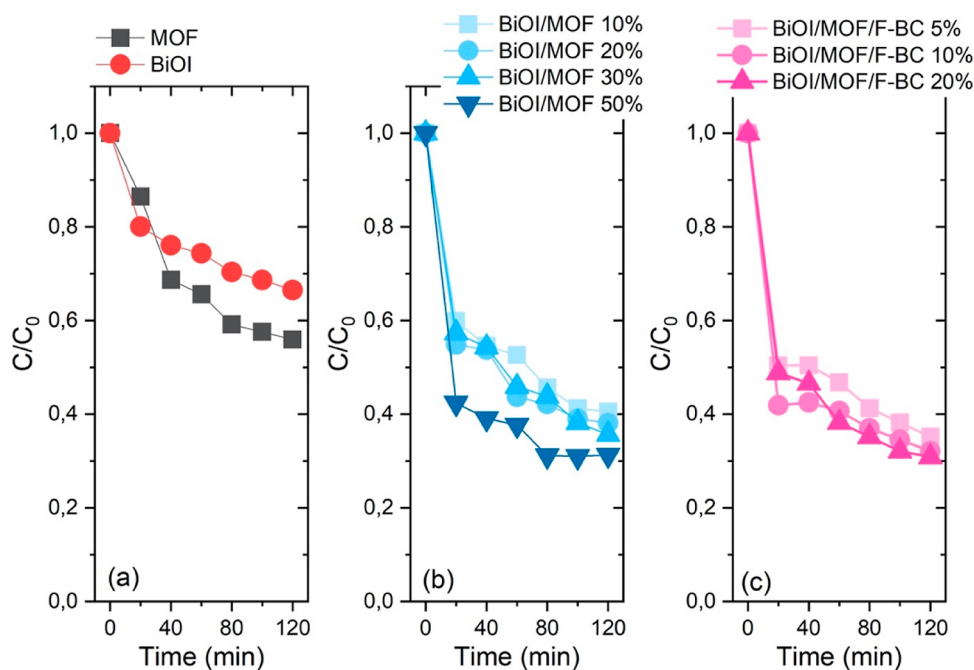
Figure 1. CIP adsorption plotted as C/C_0 for the materials under investigation. Markers are experimental points, and lines are guides for the eye. (a) Bare materials; (b) binary composites; (c) ternary composites.

however, needs a partner to support its recycling. In this sense, it has been recently proven that the $-NH_2$ functionalization of MIL-101(Fe) is a winning strategy to promote the $Fe^{III} \rightarrow Fe^{II}$ half-reaction kinetics, thus continuously generating hydroxyl radicals.[10]

Biochar, and more in general porous carbon-based materials, is gaining fame well as an adsorbent/catalytic material, alone or in combination with other catalytic systems, owing to its peculiar characteristics such as high porosity, high surface area, stability, recoverability, and possibility of insertion of functional groups.[11−15] Recent literature shows that integrating biochar in transition metal compounds is very beneficial to spurring the catalytic performance of the native materials. For instance, the *in situ* growth of $NiCo_2O_4$ nanosheets on waste biomass-derived carbon resulted in enhanced performance in the removal of phenolic compounds, attributed to the increased exposure of more M−O−M induced by the carbon material and to its intrinsic high specific surface area.[16] Biochar was also proved useful in supporting iron disulfide, grown on its surface, to activate peroxymonosulfate in the removal of tetracyclines and dyes by reducing the Fe leaching as compared to bare FeS_2.[17]

The fabrication of hybrid catalysts, consisting of materials featuring complementary skills in terms of adsorption and catalytic activity, in the attempt to create a synergistic effect, is considered a powerful strategy to introduce robust and reliable systems for water remediation.[18−22]

In the present investigation, we engineered BiOI, with a metal−organic framework (MOF), namely, NH_2-MIL-101(Fe), and with a COOH-functionalized biochar, aiming at empowering their performance as both adsorbents and photocatalysts to remove ciprofloxacin (CIP) from water.

■ RESULTS AND DISCUSSION

Adsorption of CIP under Dark. The adsorption skills of bare materials (BiOI and MOF), binary composites (BiOI/MOF-10,20,30,50%), and ternary composites with F-BC

(BiOI/MOF/F-BC-5,10,20%) were investigated under dark conditions. The course of the reaction, displayed as the relative disappearance of CIP, C/C_0, is reported in Figure 1.

Bare materials showed a moderate adsorption capability in the dark, as depicted in Figure 1 a (about 30 and 40% for BiOI and MOF, respectively, in 2 h). It should be noted that the adsorption−desorption equilibrium could not be reached after 2 h of reaction time.

The adsorption capacity of BiOI was drastically improved by the combination with NH_2-MIL-101(Fe) as a hybrid material (Figure 1b). All the binary composites showed, indeed, an excellent capability of adsorbing CIP molecules, especially the sample BiOI/MOF-50%, which could uptake 70% of the initial CIP concentration in 70 min, with 60% of it removed from the solution during the first 20 min. This makes it an excellent candidate to be used as an adsorbent for CIP residuals in water. The other three binary composites (featuring 10, 20, and 30% MOF) showed similar performance (slightly more than 60% of the initial CIP concentration was adsorbed in 120 min).

All of the ternary composites gave rise to a similar absorption capability over the long run (Figure 1c). However, the small differences observed among these samples are significant from a material composition standpoint; a plot of the amount of CIP absorbed after 120 min under dark conditions *vs* the amount of F-BC in the composites demonstrated an excellent exponential trend (Figure S1 in the Supporting Information). Similar to what was observed in the case of the binary composites, the ternary materials also display an excellent and fast CIP absorption capability (50% for the samples containing F-BC as high as 5 and 20% and about 60% for the BiOI/MOF/F-BC 10% sample in 20 min), rendering them excellent candidates as adsorbents for CIP removal from water.

We quantified the adsorption capacity at the equilibrium using a pseudo-second-order model (to which all the materials resulted to obey)

$$\frac{dq_t}{dt} = k_2(q_e - q_t)^2 \quad (1)$$

whose integrated equation is

$$q_t = \frac{q_e^2 k_2 t}{1 + q_e k_2 t} \quad (2)$$

where q_t (mg adsorbate/g adsorbent) is the absorption at a given time,[23] according to

$$q_t = \frac{(C_0 - C_t) \times V}{W} \quad (3)$$

and q_e is the adsorption at the equilibrium; C_0 (mg L^{-1}) is the initial concentration of CIP, C_t (mg L^{-1}) is the concentration of CIP at a given time, V (L) is the solvent volume, and W (g) is the mass of adsorbent used in the adsorption process. The model fitting results and pertaining parameters are reported in the Supporting Information (Figure S2 and Table S1), while Table 1 reports the obtained values for q_e and the observed kinetic constants for the adsorption process, which are also plotted as a function of the amount of MOF and F-BC in Figure 2.

Table 1. Adsorption at the Equilibrium and Observed Adsorption Kinetic Constant for the Materials under Investigation, as Retrieved from the Pseudo-Second-Order Model Applied to the Experimental Outcomes

material	q_e (mg g^{-1})	$k_2 \times 10^{-3}$ (g mg^{-1} min^{-1})
BiOI	39.31 ± 2.35	1.022 ± 0.200
BiOI/MOF 10%	68.17 ± 3.93	0.7698 ± 0.186
BiOI/MOF 20%	69.16 ± 2.83	0.9936 ± 0.221
BiOI/MOF 30%	73.53 ± 4.02	0.6739 ± 0.147
BiOI/MOF 50%	73.10 ± 2.01	1.938 ± 0.589
BiOI/MOF/F-BC 5%	70.67 ± 3.91	0.9787 ± 0.297
BiOI/MOF/F-BC 10%	70.92 ± 2.67	1.721 ± 0.619
BiOI/MOF/F-BC 20%	76.39 ± 2.38	0.9751 ± 0.186

The adsorption at equilibrium q_e was found to be an exponential function of the material's composition, for both the binary and ternary composites (Figure 2a,b). The BiOI/MOF adsorbents showed a plateau in the value of q_e for a MOF amount as high as 30%, i.e., further addition of MOF did not spur further the uptake of the CIP molecules (Figure 2a). On the other hand, a significant increase in q_e for the ternary composites (Figure 2b) was only found for the highest amount of F-BC inserted in the material (20%).

The observed kinetic constants for the adsorption process (plotted as a function of material composition in Figure 2c,d) did not give rise to any significant differences among the investigated materials; the kinetics of the process are not influenced by the material composition.

The observed findings for the adsorption process are summarized as follows: (i) the coupling of BiOI with the MOF significantly impacted the adsorption capability of the materials, almost doubling the adsorption at the equilibrium of BiOI when 30% MOF is added ($\frac{q_{e_{BiOI/MOF30\%}}}{q_{e_{BiOI}}} = 1.90$); (ii) further insertion of functionalized biochar to the binary composite did not cause a significant biochar in the value of q_e; and (iii) the kinetics of the process is not relevantly affected upon changing the material composition.

Photocatalytic Performance. The catalytic activity of bare materials (BiOI and MOF), binary composites (BiOI/MOF-10,20,30,50%), and ternary composites with F-BC was investigated under simulated solar light (the reaction courses are shown in Figure 3).

The catalytic activity of BiOI and MOF upon simulated solar light (Figure 3a) was rather poor, with BiOI overperforming the MOF by 10% in 3 h. Overall, only 30% of the initial CIP concentration was removed in a rather long reaction time (180 min).

On the contrary, the binary compounds showed a good capability of degrading CIP (Figure 3b); the addition of MOF to BiOI resulted in enhanced catalytic performance, which correlated very well with the percentage of MOF in the composites according to an exponential trend up to 120 min reaction time (see Figure S3 in the Supporting Information), after which the binary composites featuring 30% MOF overperformed all the homologues.

We monitored the reaction for 180 min, verifying the following: (i) the insertion of 10% MOF results in a fair CIP degradation at long reaction times, but the reaction kinetics is the slowest of the investigated batch; (ii) at long reaction times, the composites featuring 10 and 20% MOF did not significantly differ in terms of their CIP degradation capability; (iii) the composites with 30 and 50% MOF content display similar catalytic performance, but over the long run, the former is capable of removing more antibiotics (it was then chosen as the base material to synthesize the ternary composites).

Upon simulated solar light irradiation, all of the ternary composites showed an excellent capability of degrading CIP (Figure 3c): after 1 h, between 40 and 60% of the initial CIP amount was removed. At longer reaction times (180 min), we observed the disappearance of almost 95% when the process was catalyzed by the sample containing 10% of F-BC (the best of the batch, whose recyclability was tested as well; see Figure S4 in the Supporting Information), while the other two catalysts could remove between 75% (BiOI/MOF/F-BC 20%) and 83% (BiOI/MOF/F-BC 5%).

Catalytic results are summarized in Table 2.

A deeper analysis of the reaction courses for the bare materials (BiOI and MOF) and the best-performing composites (BiOI/MOF 30% and BiOI/MOF/F-BC 10%) allowed us to observe that different catalytic materials obey different reaction mechanisms (Figure 4 and Table S2 in the Supporting Information).

Specifically, we observed a well-behaved linear behavior in the case of CIP degradation degraded by pure BiOI (Figure 4a) which, however, appears to be associated with a pseudo zero-order reaction, since C/C_0 vs time is also linear (see Figure S5 in the Supporting Information).

A reaction order higher than one was instead found for the reaction catalyzed with bare MOF (Figure 4b), which followed a sigmoidal trend, highlighting the occurrence of an autocatalytic reaction. This indicates that NH$_2$-MIL-101(Fe) is an active catalyst, although sloppy, for the degradation of CIP also under dark conditions. This was expected from previous literature, where the material was used to catalyze the degradation of several molecular targets, through the activation of H$_2$O$_2$, without the need to be light-activated.[6,8,10] The presence of reaction products in the reaction mixture when the light was switched ON promoted the reaction at early reaction times (up to 90 min), as is visible in Figure 3a, during which the MOF slightly outperformed bare BiOI.
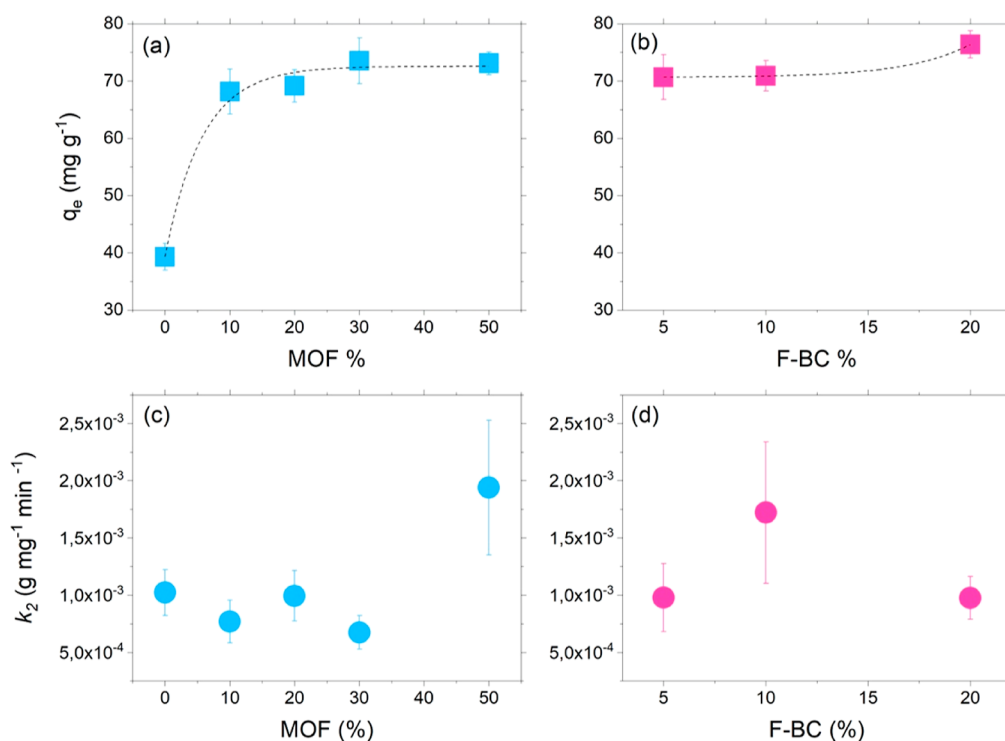
Figure 2. (a,b) Adsorption at the equilibrium q_e and (c,d) observed kinetic constants for the adsorption process for the materials under investigation as a function of the content of MOF and F-BC.
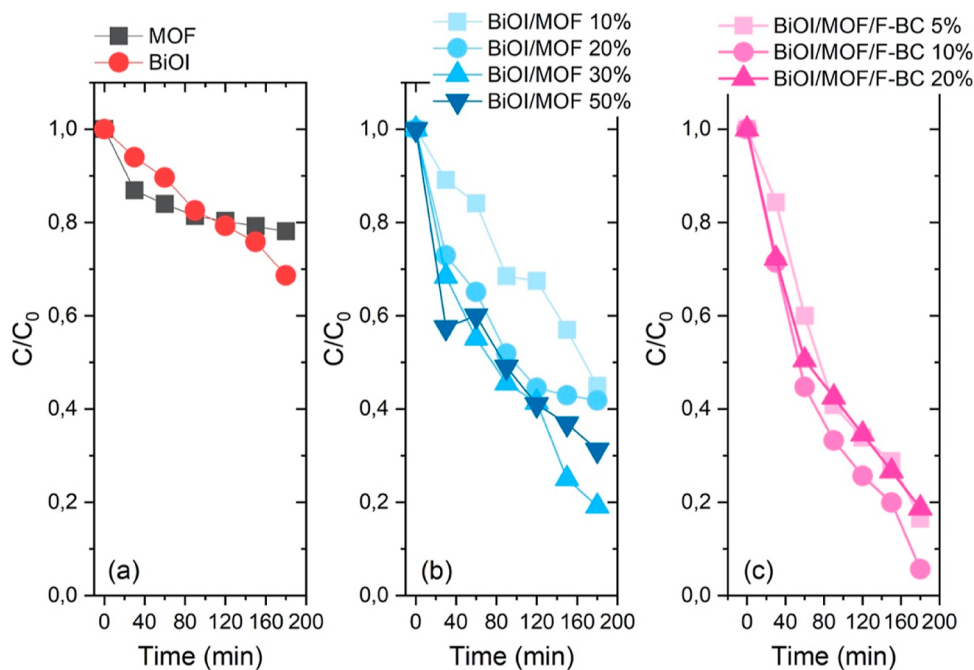

Figure 3. Reaction course for the CIP degradation under simulated solar light for the investigated materials: (a) bare materials; (b) binary composites; (c) ternary composites. Markers are experimental points, and lines are guide for the eye.

The reaction supported by binary composite BiOI/MOF 30% displayed pseudo-first-order kinetics (Figure 4c). It is interesting to remark that the absence of a sigmoidal trend indicates that MOF is no longer active as a catalyst under dark when combined with BiOI, suggesting that the interaction between the Fe(III)/Fe(II) species in the MOF and the BiOI is favored, as compared with the interaction with the MOF with the surrounding environment (*i.e.*, the CIP molecules in

the reaction mixture). Furthermore, the catalytic behavior of the binary composite is changed, as compared with that of the bare materials, resulting in a different reaction order, suggesting a different reaction mechanism, induced by the different nature of the catalytic material.

When the ternary composite BiOI/MOF/F-BC 10% was used as the catalyst, a more complex behavior was identified (Figure 4d). Indeed, the semilog plot of the reaction course

Table 2. Summary of the Photocatalytic Results

material	CIP degradation under light @ 180 min (%)
BiOI	31.3
MOF	21.9
BiOI/MOF 10%	55.0
BiOI/MOF 20%	58.2
BiOI/MOF 30%	81.9
BiOI/MOF 50%	68.8
BiOI/MOF/F-BC 5%	83.5
BiOI/MOF/F-BC 10%	94.4
BiOI/MOF/F-BC 20%	75.6

under light irradiation showed two different regimes: a linear trend (pseudo-first-order kinetics) up to 90 min reaction, followed by an exponential (higher kinetic order) trend. This change is attributed to the presence of the functionalized biochar; the generation of acidic group resulted in the possibility of hydrogen-bonding CIP thus promoting its degradation.[12]

Fitting equations and R^2 values are reported in Table S2 in the Supporting Information.

Influence of pH Conditions on CIP Degradation. CIP degradation, photocatalyzed by the ternary composite BiOI/MOF/F-BC 10%, was studied under different acidic/alkaline conditions (the results are shown in Figure 5). Forcing a certain pH implies imposing a change in the CIP form, with its acidic dissociation constants equal to $pK_{a1(COOH)}$ = 6.09 and $pK_{a2(NH)}$ = 8.74.

It was previously reported that strong alkaline conditions favor CIP degradation, possibly due to an easier UV excitation of the antibiotics.[24] We observed the same in the present study (Figure 5a); in an acidic pH, with CIP fully protonated, the reaction was slow and poorly efficient, and less than 30% of the initial CIP amount (10 ppm) was removed. Increasing the pH

up to and beyond 9 (with both the carboxylic group and the NH on the piperazinyl ring deprotonated) resulted in a much faster and more efficient reaction (especially at initial times) and complete CIP removal after 150 min. The comparison of the outcomes for the reaction carried out at pH 9 and 11 highlighted small but significant differences in terms of the amount of degraded CIP at the same reaction time (Figure 5b). This finding indicates that not only the form of CIP is relevant to its removal but also the concentration of the hydroxyl ions in the solution (see the following section on the reaction carried out in the presence of ROS scavengers).

Identification of the Reactive Oxidizing Species. We finally investigated the photodegradation of CIP in the presence of different scavenging agents, specifically potassium iodide (trapping holes), p-benzoquinone (trapping the superoxide anion radical), and isopropyl alcohol (trapping the hydroxyl radical). The outcomes are reported in Figure 6. All trapped species seemed to have a role in the CIP degradation catalyzed under light irradiation by the ternary composite, again highlighting the complexity of this reaction. However, this role is played to different extent by different species. The analysis of the course of the reaction (Figure 6a) showed that the photogenerated holes are not the main species degrading CIP; their removal affects the course reaction only at prolonged reaction times (>90 min). Their recombination rate with the photogenerated electrons is possibly faster than the redox processes involved in CIP destruction. This was also confirmed by the fact that we could not observe any clear correlation between the absorption features of the materials and the amount of CIP degradation.

The removal of superoxide anion radical, on the other hand, affected more significantly the degradation of CIP over the time, and we observed only a 60% disappearance of the molecule in 3 h of reaction time.
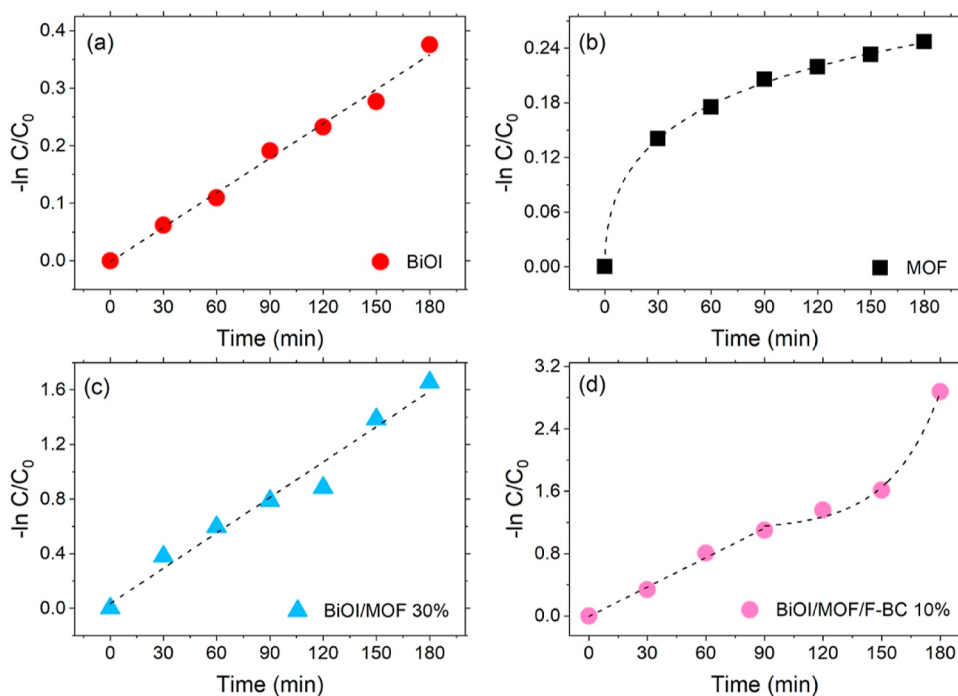

Figure 4. Reaction course for the degradation of CIP upon light irradiation plotted as $-\ln(C/C_0)$ for pure BiOI (a), BiOI (b), BiOI/MOF-30% (c), and BiOI/MOF/F-BC-10% (d). Markers are experimental points, and lines are fitting curves.
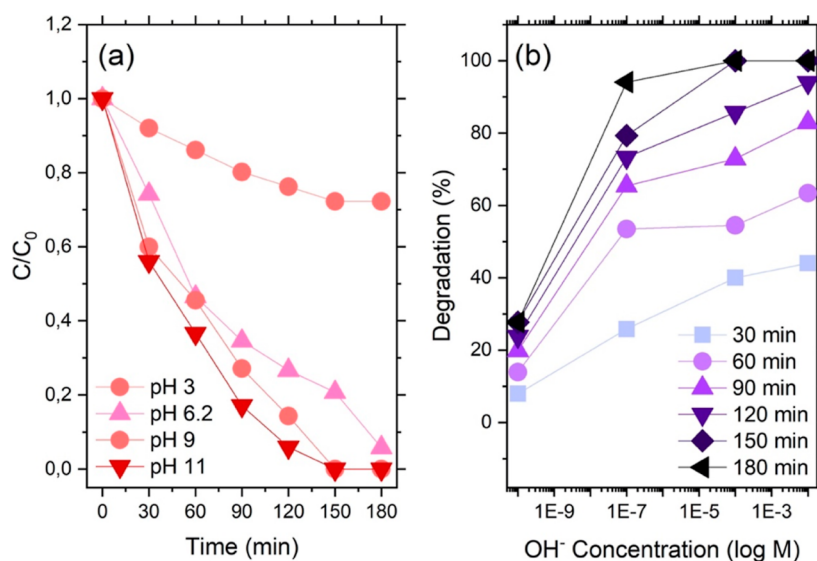
Figure 5. (a) Reaction course plotted as C/C_0 vs time for the degradation of CIP as a function of the reaction mixture pH (pH = 6.2 corresponds to the CIP autodissociation). (b) Percentage of degraded CIP vs OH^- concentration at different reaction times.
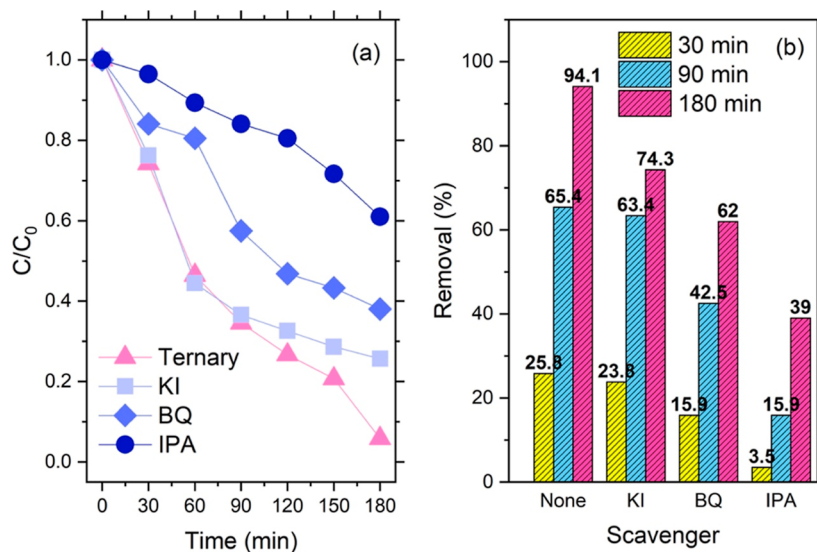

Figure 6. (a) Reaction course for the photodegradation of CIP under the action of different trapping agents. (b) Comparison of CIP removal at different reaction times for different trapping agents.

Finally, we verified that the hydroxyl radicals played the most critical role in CIP removal. When IPA was added to the reaction mixture, the process slowed and significantly suppressed, indicating that these species dominate the redox reaction in charge of CIP degradation. A visual analysis of the relative role played by different trapping agents is provided in Figure 6b.

In an attempt to correlate the observed behaviors as adsorbents and photocatalysts with materials' physical features, we analyzed the physical and chemical features of the bare materials (BiOI and the MOF) and the composites displaying the best functional performance (BiOI/MOF 30% and BiOI/MOF/F-BC 10%).

Structural and Morphological Characterization. X-ray diffraction (XRD) patterns of the materials under investigation are reported in Figure 7. We focused our analysis on the possible changes induced in the BiOI structure during the *in situ* fabrication of the binary and ternary composites. Bare BiOI

showed the reflections of planes (101), (102), (110), (200), (212) at 24.32, 29.2, 31.76, 45.53, and 54.85°, respectively (JCPDS card no. 00-73-2062), displaying the expected tetragonal structure. The same reflections are found in the XRD patterns of the composites, although slightly changed in terms of width and intensity, indicating that the fabrication process modified the native structure of BiOI. Reflections pertaining to the MOF are not visible in the analyzed composites (with the exception of a peak centered at 52.74° in the binary composite with the highest amount of MOF, *i.e.* 50%), indicating that BiOI structurally dominates the diffraction patterns. This was previously observed in the literature[7,25] and can be ascribed to a high degree of dispersion of the MOF.

The XRD pattern of NH_2-MIL-101(Fe) was in agreement with the literature.[26,27] XRD analysis of the oxidized biochar (reported in Figure S6 in the Supporting Information) revealed the presence of two peaks, centered at 22.7 and 41.9°, ascribed
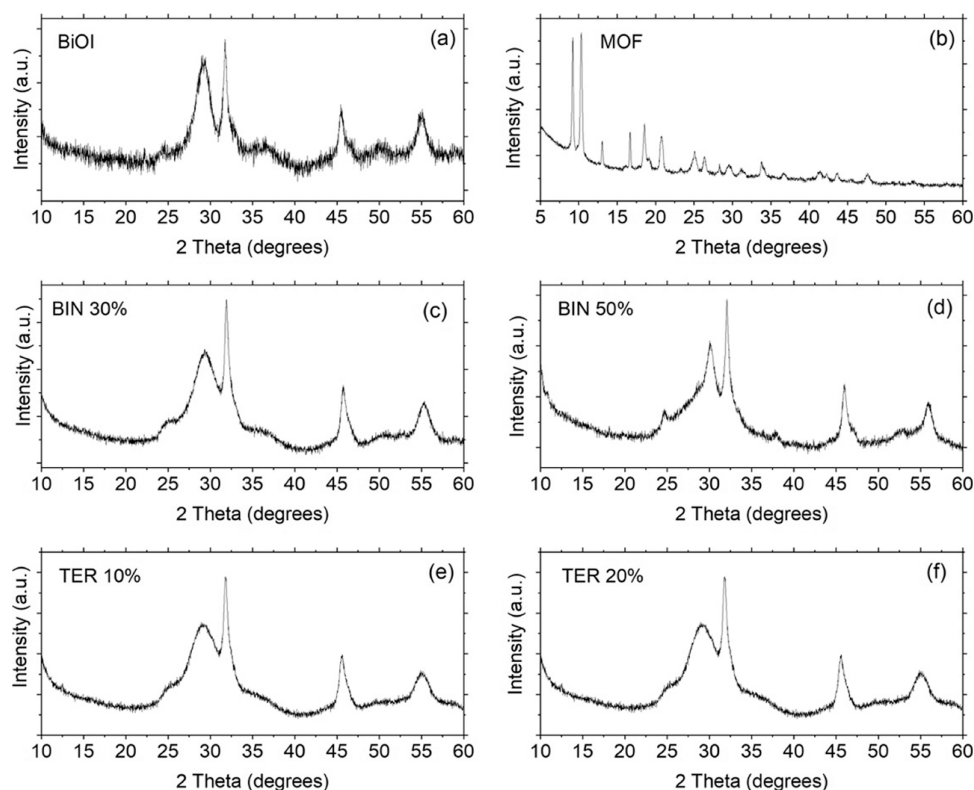
Figure 7. XRD patterns of the materials under investigation. (a) BiOI; (b) MOF; (c) BiOI/MOF 30%; (d) BiOI/MOF 50%; (e) BiOI/MOF/F-BC 10%; and (f): BiOI/MOF/F-BC 20%.

to the plane indexes (002) and (100), respectively. Both peaks are asymmetric, rather broad, and feature small intensity. The asymmetry of the (002) reflection is associated with the parallel packing of the carbon layers and indicates the presence of amorphous and aliphatic structures.[28] The (100) reflection is due to the diffraction of hexagonal graphene carbons.[29]

The quantitative analysis of the structural parameters of BiOI considered bare and in the composites (reported in Tables 3 and S2 in the Supporting Information) showed the

Table 3. Structural Parameters (Unit Cell Sizes and Average Crystallite Size) Are Retrieved from XRD Analysis[a]

material	unit cell sizes (Å)		average crystallite size (nm)
	a and b	c	
BiOI	3.99	9.32	13.3
BIN 30%	3.97	9.40	11.0
BIN 50%	3.95	9.00	12.5
TER 10%	3.98	9.83	4.97
TER 20%	3.98	9.83	4.97

[a]The average crystallite size D was evaluated using Debye−Scherrer analysis: $D = \frac{K\lambda}{\beta \cos \theta}$, where K is the shape factor (taken as 0.94), λ the X-ray wavelength (1.54178 Å), β the full width at half-maximum (fwhm) of the reflection used in the calculation, and θ the reflection angle.

following: (i) the native structure of BiOI is reproduced in all the composite materials, with small differences in the unit cell sizes; (ii) the interplanar distance d is found unchanged by comparison between pure BiOI and BiOI in the composites; (iii) different amounts of MOF added to BiOI cause a reduction in its average crystallite size of about 17% (MOF

30%) and 6% (MOF 50%); (iv) the decrease in the average crystallite size is much higher when F-BC is inserted in the composites (55%), but different amounts of F-BC resulted in the same average crystallite size. This finding indicates that the amount of MOF (the same in both ternary composites) rules the formation of BiOI. Our hypothesis is that we are herein observing an electrostatic interaction between the BiOI precursor and the MOF [possibly between the negatively charged oxygen atoms in $Bi(NO_3)_3$ and the positively charged $-NH_2$ groups in NH_2-MIL-101(Fe)], which dictates the subsequent formation of BiOI.

Figure 8 reports the scanning electron microscopy (SEM) images of the samples under investigation. BiOI featured hierarchical 3D microspheres with an average diameter of 1.6 ± 0.2 μm (Figure 8a). As-synthesized MOF displayed a hexagonal microspindle shape, with length calculated around 1−3 μm (Figure 8b). The functionalized biochar showed a honeycomb-like morphology (Figure 8c), with pore sizes exceeding 5 μm. A porous structure is commonly reported for biochars,[30] which should enhance the adsorption of organic molecules, thus spurring the subsequent catalytic degradation, thanks to a proximity effect.

Both the binary and ternary composites showed the incorporation of MOF as well as of F-BC in the BiOI structures (Figure 8d,e), which retained the same morphology they displayed when synthesized on their own.

UV−Vis Absorption Spectroscopy. The interaction with light was studied by UV−vis absorption spectroscopy. This property is relevant in semiconductor-supported photo-catalysts, and extension of light absorption should indeed enhance the photogeneration of charges useful for subsequent redox reactions, responsible for pollutant degradation.
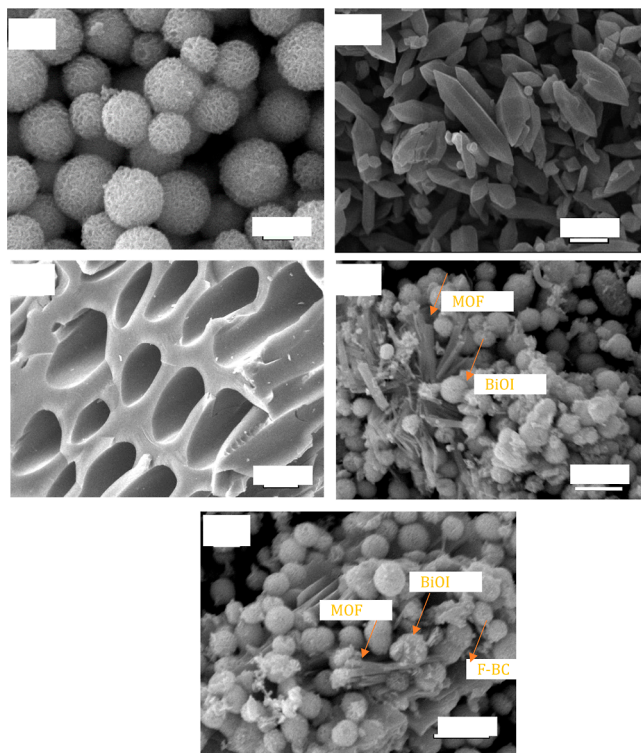
Figure 8. SEM images of the prepared materials. (a) BiOI, (b) MOF, (c) F-BC, (d) BiOI/MOF-30%, (e) BiOI/MOF/F-BC-10%.

The diffuse reflectance spectra of the prepared materials are shown in Figure 9a. All of the materials showed a high absorption up to around 500 nm, which then decreased to different amounts, depending on the specific compound. The addition of both MOF and F-BC extended light absorption to higher wavelengths as compared with that of bare BiOI.

The optical energy gap (E_g) of the materials was calculated from the absorption data (Tauc plot shown in Figure 9b and values reported in Table 4). A significant reduction in the E_g was observed for the composite materials, compared to bare BiOI (1.84 eV); the optical energy gap was found to be as high

Table 4. Optical Energy Gap as Retrieved from Absorption Measurements

material	energy gap (eV)
BiOI	1.84
MOF	1.10
BiOI/MOF 30%	1.52
BiOI/MOF/F-BC 10%	1.61

as 1.52 eV for the binary material and 1.61 eV for the ternary composite.

Fourier Transform Infrared Spectroscopy. Fourier transform infrared (FTIR) spectroscopy was applied to investigate the formation of the composites by the comparative analysis of their vibrations with the signals pertaining to the bare materials (Figure 10).

The success of the acidic functionalization of the biochar was confirmed by the presence of a very intense and extremely broad peak centered at 1895 cm^{-1}, ascribed to the C=O stretching of the carboxylic groups. Signals centered at 1650 and 1493 cm^{-1} were attributed to the asymmetric and symmetric stretching of the O–C=O groups, respectively.

BiOI infrared spectrum presents the peak typically ascribed to the Bi–O stretching vibration centered at 520.7 cm^{-1}, together with an asymmetric sharp and rather intense signal at 1384.8 cm^{-1}, due to the overlapping of symmetric and asymmetric stretching of the Bi–I bond.[7,31] The analysis of the infrared spectrum of BiOI also revealed the presence of water molecules (H$_2$O bending at 1620 cm^{-1} and O–H stretching at 3420 cm^{-1}) and residuals of ethylene glycol from the synthesis (fingerprint triplet pertaining to the CH$_2$ stretching at 2970, 2920, and 2850 cm^{-1} and doublet at 1078 and 1047 cm^{-1}). Ethylene glycol residuals were also identified in the spectra of the binary and ternary composites.

The FTIR spectrum of MOF clearly showed the vibrations of amines (3462, 3336.7, 3184.3 cm^{-1} N–H stretch; 1575 cm^{-1} N–H bending; 1257.5 cm^{-1} C–N stretching; 769.6 cm^{-1} N–H wagging), as well as the peaks pertaining to the asymmetric and symmetric COO$^-$ stretching (1658.7 and 1579.6, 1427 and 1393 cm^{-1}, respectively). The breathing modes of the phenyl rings are also visible (623 cm^{-1}), partly
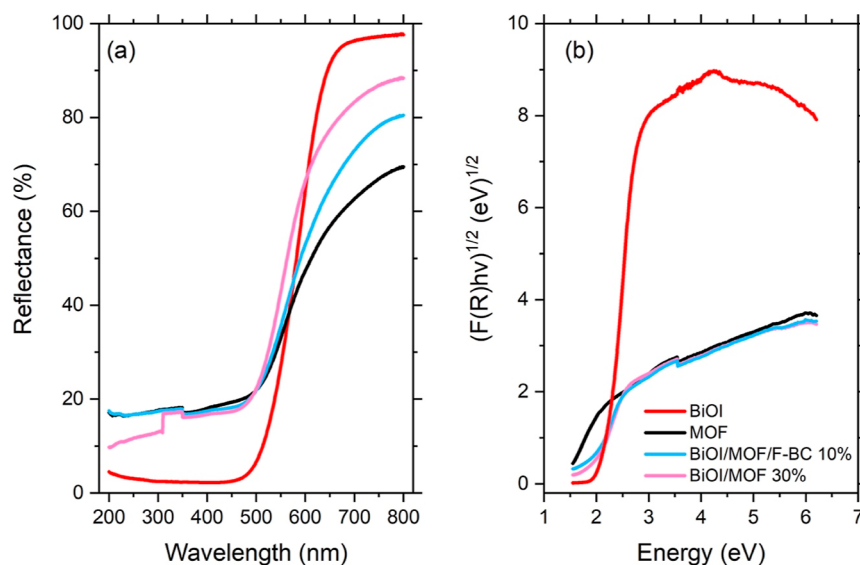

Figure 9. UV–vis absorption spectra (a) and Tauc plots (b) of the prepared materials.
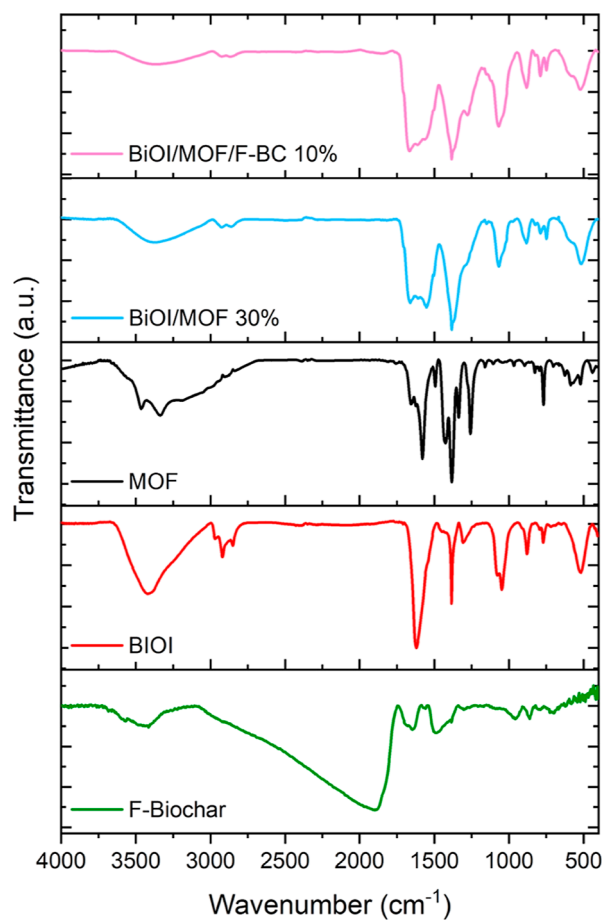
Figure 10. FTIR spectra of materials under investigation.

these vibrations from the bare materials suggests an interaction between the iron and the bismuth species in the composites, which would account for their combined action in photocatalysis.

Overlapping of the C−N stretching with the symmetric COO^- stretching results in an unresolved triplet spanning from 1253 to 1382 cm^{-1}, while the asymmetric COO^- stretching is still well visible at higher wavenumbers (1551 to 1660 cm^{-1}). Around 3370 cm^{-1}, the combined stretching of O−H and N−H is present. In the ternary composite, a further multiplet is also present (around 1850 cm^{-1}), ascribed to the C=O stretching of the carboxylic functions produced in the functionalized biochar.

Summarizing the above, FTIR analysis provided further proof of the formation of the desired binary and ternary composites, featuring a combined structure in which BiOI was coupled with the MOF and the biochar.

Correlating Material Characteristics with Functional Performance. We analyzed the performance of the materials in terms of their adsorption at the equilibrium and CIP degradation, focusing on BiOI as the main catalytic species, as a function of the crystallite sizes and the calculated optical band gap (Figure 11). We could observe an obvious dependence of both adsorption and CIP degradation on the crystallite sizes; the lower the latter is, the better the performance (Figure 11a,b).

This finding is a common claim in the literature analyzing the catalytic and photocatalytic performance of polycrystalline, nanostructured semiconductors; smaller crystallite sizes would enhance the number of catalytically active sites, thus spurring the degradation of targeted pollutants. No trend was found correlating the degradation of CIP under simulated solar light with the optical bandgap of the materials, and the modulation of this parameter does not affect the CIP removal from water. Eventually, this means that the modulation of light absorption plays a minor role in photocatalysis, surpassed by the structural features of materials. This finds confirmation also in the catalytic tests supported by the ternary composite and carried out in the presence of ROS scavengers; the photogenerated holes are the species playing the smallest role in degrading CIP.
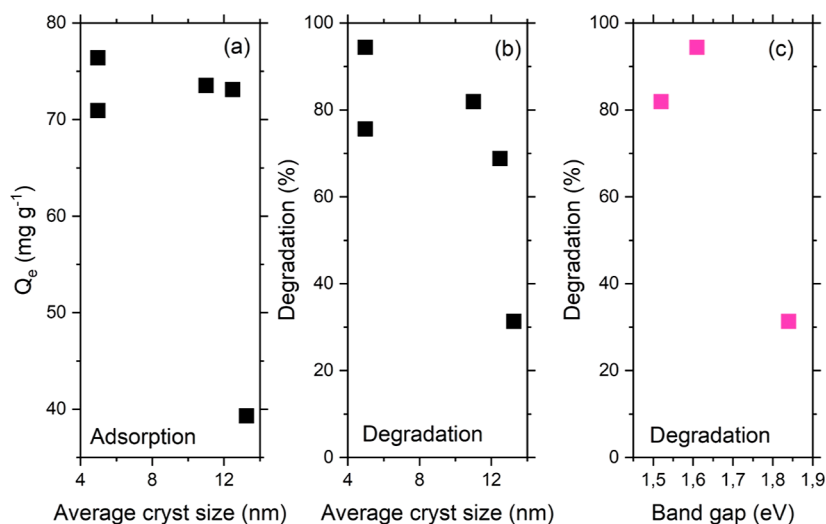
overlapping with the stretching of Fe−O (586 cm^{-1}), which also presents a signal at 439 cm^{-1}.

Several of these vibrations appear in the FTIR spectra of the binary and ternary composites as well; in both samples, an unresolved doublet is present at 520 and 578 cm^{-1}, and this signal is the combination of the vibrations from the BiOI and the Fe−O bonds in the MOF. The loss of a clear identity of

Figure 11. Dependence of adsorption at equilibrium and CIP photodegradation (at 180 min) as a function of (a,b) the average crystallite size and (c) the optical band gap.
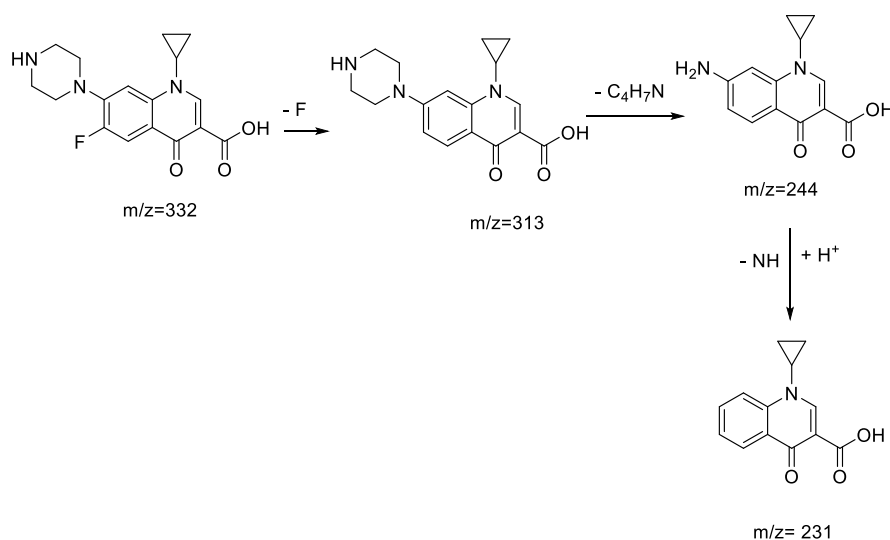
Figure 12. Proposed mechanism for CIP degradation catalyzed by BiOI/MOF/F-BC 10%.

High-Performance Liquid Chromatography Coupled with Mass Spectrometry. We employed high-performance liquid chromatography—mass spectrometry (HPLC—MS) analysis to investigate the reaction mixtures and ascertain that the products generated in the CIP photodegradation are catalyzed by 10% BiOI/MOF/F-BC under different pH conditions. We then identified a pH-dependent degradation of the CIP (as demonstrated in Figure S7 in the Supporting Information), which has been previously documented in the literature,[32−35] validating our research findings.

The predominant photolytic pathway for CIP in acidic media involves oxidation of the piperazine ring and cleavage of the C—F bond.[32,34] As a result of these reactions, a number of intermediates can be formed, including those with m/z values of 186, 205, and 217. These intermediates can undergo subsequent reactions and degradation pathways, as documented in the existing literature.[35,36] The above masses were detected for the reaction mixture at pH 3 with BiOI/MOF/F-BC 10%, albeit with low intensity, indicating the possibility that the same mechanism is followed. The specific oxidation products formed during the degradation of piperazine-containing compounds may vary depending on the specific conditions and the presence of other reactive species. Moreover, when the reaction is carried out at pH 3, a compound featuring a parent ion with m/z of 332 is observed, indicating incomplete degradation of CIP.

A comparable degradation pathway was observed even at higher pH values (6.2, 9, and 11), resulting in the complete degradation of CIP into fragments with low molecular masses.

Specifically, the presence of m/z = 231 was detected at pH = 6.2 and 9, while m/z = 245 was detected at pH = 11, indicating the involvement of the following degradation pathway (Figure 12).[36]

It is worth noting that some intermediates were not detected at different pH values, e.g., m/z = 313 at pH 6.2 and 9; and m/z = 231 and 313 at pH = 11.

The degradation of CIP is favored in highly alkaline media. The presence of alkaline conditions promotes the formation of hydroxyl radicals through reactions with hydroxide ions and other reactive species. Hydroxyl radicals are known for their high reactivity and play a crucial role in initiating the degradation of CIP.

These results are consistent with the photocatalytic degradation finding, which indicates partial degradation of CIP at pH 3 and complete degradation at higher pH values (pH = 6.2−11). In addition, the results are also consistent with what was observed in the test carried out with scavenging agents, indicating the efficiency of superoxide anion radicals and hydroxyl radicals in CIP removal at higher pH values.

■ CONCLUSIONS

A batch of binary and ternary compounds based on BiOI were synthesized, aimed at empowering this semiconductor photocatalyst with a MOF and a functionalized biochar. BiOI was thus combined with different amounts of NH₂-MIL-101, and the best photocatalyst of this batch was used as the base material for the synthesis of a series of ternary hybrid composites with a COOH-functionalized biochar. All of the materials were then tested as adsorbers and photocatalysts for the removal of CIP from water.

The experimental outcomes showed that (i) the combination with MOF and F-BC drastically enhanced BiOI properties as both adsorber and photocatalyst; (ii) the fabricated composites are interesting adsorbers and photocatalysts for the removal of CIP from water; and (iii) there is a clear dependence between the adsorption at the equilibrium and the amount of degraded CIP upon simulated solar light irradiation on BiOI average crystallite size, which results in the main parameter determining the performance of the investigated materials. The role of NH₂-MIL-101(Fe) is to enhance the adsorption capability of the materials, as observed through quantification of the adsorption at equilibrium; the induced proximity effect subsequently spurs CIP degradation under light excitation. The *in situ* addition of biochar, then, causes a significant decrease of BiOI crystallite sizes, which further promotes the catalytic action of the semiconductor. The combined action of these two chemicals on BiOI results in the empowerment of its functional performance.

The best photocatalyst of the investigated batch was tested at different pH conditions: these tests resulted in different amounts of CIP being removed from the original solution, as expected. However, the interesting outcome was that increasing the pH of the solution (compared to the pH induced by the spontaneous CIP dissociation in water) did not

Scheme 1. Synthesis of Ternary Composites BiOI/MOF/F-BC
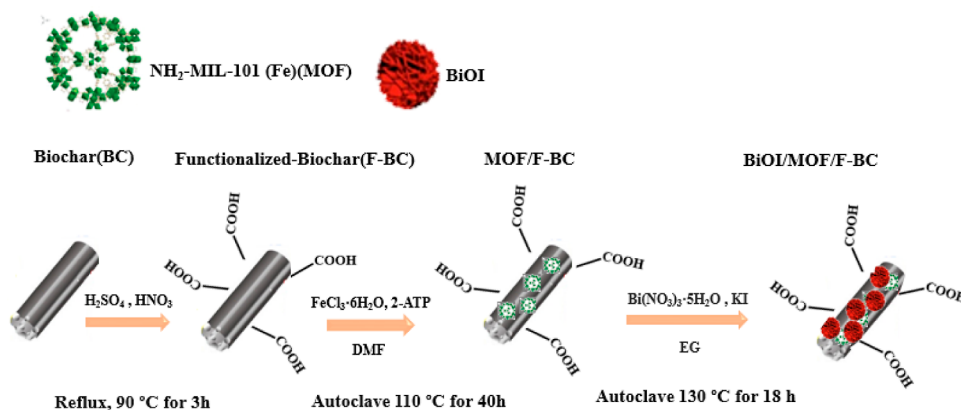
affect the amount of CIP degraded at prolonged reaction times (180 min).

The photocatalytic tests with scavenging agents showed that several ROS are involved in CIP degradation, which is again confirmed as a complex process with kinetics driven in different ways by different ROS. This further confirms that in real scenarios, the best strategy to remediate waters is the combination of different techniques.[37]

The present investigation shows that the fabrication of hybrid composites is a winning strategy to enhance the performance of BiOI as both an adsorber and a photocatalyst for CIP removal, indicating, however, that crystallite sizes command the overall process.

■ METHODS

Material Synthesis. For the synthesis of materials, precursors from Sigma-Aldrich (ACS reagent, ≥98%) were used as-received, without any additional purification.

Synthesis of BiOI. $Bi(NO_3)_3 \cdot 5H_2O$ (0.98 g) was dissolved in 15 mL of ethylene glycol (EG) under vigorous stirring for 30 min. In another beaker, KI (0.33 g) was dissolved in 15 mL of EG under stirring for 30 min. The obtained KI solution was added dropwise to the $Bi(NO_3)_3 \cdot 5H_2O$ solution under continuous stirring for 30 min. The reaction mixture was then transferred to a stainless-steel autoclave lined with Teflon and heated at 130 °C for 18 h. The precipitate was washed three times with distilled water and ethanol and, subsequently, dried in an oven at 60 °C. For a detailed discussion of the synthesis protocol, the reader is referred to ref 24.

Synthesis of NH₂-MIL-101(Fe)(MOF). 0.89 g of $FeCl_3 \cdot 6H_2O$ and 0.29 g of 2-aminoterephthalic acid (2-ATP) were separately dissolved in 20 mL of N,N-dimethylformamide, under continuous stirring for 20 min. The $FeCl_3 \cdot 6H_2O$ solution was added to the 2-ATP solution and kept under magnetic stirring for 2 h. The reaction mixture was then sealed in a Teflon-lined autoclave and heated in an oven for 40 h at 110 °C. The product was washed with ethanol and distilled water and eventually dried overnight in an oven at 80 °C in an ambient atmosphere.

Synthesis of Binary Composites (BiOI/MOF-10,20,30,50%). 0.98 g of $Bi(NO_3)_3 \cdot H_2O$ (0.98 g) was inserted into 15 mL of ethylene glycol and added to previously prepared MOF dispersions in 10 mL of the same solvent (appropriate amounts of MOF were used to reach a final composition of the binary composites, with the BiOI to MOF ratio as high as 10, 20, 30, and 50% w/w). Each reaction

mixture was stirred for 2 h. Thereafter, KI (0.33 g) was dissolved in 15 mL of EG and added dropwise to the reaction mixture under stirring for 2 h. The final mixture was loaded into a Teflon-line autoclave and heated for 18 h in an oven at 130 °C. The product underwent a thorough cleaning process involving the use of ethanol and distilled water for washing. Subsequently, it was carefully dried overnight in an oven set at 80 °C, maintaining an ambient atmosphere.

Acidic Oxidation of Biochar. The biochar used in the present work was prepared according to a previously published method.[38]

The functionalization of biochar was accomplished as follows: HNO_3-40% and H_2SO_4-60% were mixed together with the 1/3(v/v) ratio and added to 200 mL of water. 2.5 g of biochar was added to the above solution and kept under reflux at 70 °C for 6 h. The oxidized biochar was washed with distilled water for 2 h until the pH of the solution reached a neutral condition and dried in an oven at 80 °C overnight.

Synthesis of Ternary Composites (BiOI/MOF/F-BC-5,10,20%). Functionalized biochar was dispersed in 10 mL of DMF and sonicated for 1 h. The amounts of F-BC were calculated to reach a final composition of the ternary composites with a BiOI/F-BC w/w ratio as high as 5, 10, and 20%, respectively. The ratio of BiOI/MOF was kept at 30% with respect to the weight amount of MOF to BiOI.

$FeCl_3 \cdot 6H_2O$ (0.89 g) was added to the F-BC dispersions, which were stirred for 40 min, and 2-ATP (0.29 g) was then added. After 1 h of stirring, the reaction mixture was placed in an oven for 40 h at 110 °C. The obtained brown powder was dispersed in 15 mL of EG and sonicated for 20 min. 0.98 g of $Bi(NO_3)_3 \cdot 5H_2O$ was then added to the dispersion, which was stirred for 1 h before adding dropwise (2 h) KI (0.33 g) dissolved in 15 mL of EG. The resulting precursor suspension was loaded into a Teflon-lined stainless-steel autoclave and kept at 130 °C for 18 h. Finally, the resulting material was washed and inserted into a vacuum oven overnight at 80 °C (the synthesis is shown in Scheme 1).

Material Characterization. XRD analysis was performed in a PANalytical Empyrean instrument equipped with a PIXcel3D detector using Cu Kα radiation at 40 keV and 45 mA settings.

SEM was carried out in a JSM-IT300 scanning electron microscope equipped with an energy-dispersive X-ray detector (EDX).

FTIR spectra were recorded in a Bruker VERTEX 80v in the range 4000−400 cm^{-1} in transmittance mode.

Optical absorption spectroscopy was carried out in an Agilent Cary 5000 spectrophotometer.

Brunauer−Emmett−Teller (BET) of materials was investigated with a Micromeritics Gemini V 2390 apparatus (Micromeritics, Norcross GA, USA). The samples were degassed under vacuum (1×10^{-4} Pa) at 90 °C for 24 h before measurement.

Thermogravimetric analysis (TGA) was carried out through an STA 449C Jupiter (NETZSCH, Germany) instrument. Each sample (5−10 mg) was heated from 25 to 700 °C at a rate of 10 °C min^{-1} under an Ar flow.

Adsorption Tests. Ten mg of each adsorber species was added to 100 mL of CIP solution (10 ppm). The mixtures were kept in the dark and vigorously stirred for 120 min. Aliquots were withdrawn at fixed time intervals and analyzed with the help of spectrophotometry (Agilent Cary 5000 spectrophotometer) to determine the CIP disappearance by monitoring the evolution of the absorption peak centered at 276 nm.

Photocatalytic Tests. A LOT-QD solar simulator was used as the light source (AM 1.5G spectrum at 1 sun intensity, calibrated with a silicon reference cell). Ten mg of each catalyst was added to a 10 ppm CIP aqueous solution. Aliquots of the reaction mixtures were extracted at specific times and analyzed through spectrophotometry (Agilent Cary 5000 spectrophotometer) after centrifugation. CIP concentration was quantified by monitoring the evolution of the peak centered at 276 nm.

For the tests carried out under different pH conditions, HCl and NaOH were added to the solutions in appropriate amounts to reach pH 3, 9, and 11.

To analyze the role played by ROS in the photodegradation of CIP, 2 mM of various scavengers potassium iodide (KI, h$^+$), *p*-benzoquinone (BQ, trapping the $^{\bullet}O_2^{-}$), and isopropyl alcohol (IPA, $^{\bullet}OH$) was added, following the same procedure as described in the photodegradation test.

High-Performance Liquid Chromatography−Mass Spectrometry. For HPLC−MS analysis, an Agilent 6130 quadrupole LC/MS instrument was employed with an electrospray ion source in positive ion mode. An adequate amount of the reaction mixture (2 μL) was injected into the HPLC column (C18, 50×3 mm with a 3 μm particle size and 100 Å pore size). In the mobile phase, a combination of water (solvent A) and acetonitrile (solvent B) (70:30) was used, both solvents containing 0.1% (v/v) formic acid.

■ ASSOCIATED CONTENT

Ⓢ Supporting Information

The Supporting Information is available free of charge at https://pubs.acs.org/doi/10.1021/acsomega.3c06243.

> Adsorption under dark *vs* F-BC content; fitting of adsorption process and related parameters; photodegradation *vs* MOF content; recyclability of BiOI/MOF/F-BC 10%; fitting parameters for the reaction courses; fitting of photodegradation supported by pure BiOI; structural parameters; XRD pattern of F-BC; and HPLC data (PDF)

■ AUTHOR INFORMATION

Corresponding Author

Isabella Concina − *Department of Engineering Sciences and Mathematics, Luleå University of Technology, 98187 Luleå,* Sweden; ⓞ orcid.org/0000-0003-1785-7177; Email: isabella.concina@ltu.se

Authors

Sepideh G. Khasevani − *Department of Engineering Sciences and Mathematics, Luleå University of Technology, 98187 Luleå, Sweden*

Dariush Nikjoo − *Department of Engineering Sciences and Mathematics, Luleå University of Technology, 98187 Luleå, Sweden*

Cécile Chaxel − *Department of Engineering Sciences and Mathematics, Luleå University of Technology, 98187 Luleå, Sweden*

Kentaro Umeki − *Department of Engineering Sciences and Mathematics, Luleå University of Technology, 98187 Luleå, Sweden;* ⓞ orcid.org/0000-0001-6081-5736

Shokat Sarmad − *Wallenberg Wood Science Center, Department of Chemistry Technical Chemistry, Department of Chemistry, Chemical-Biological Centre, Umeå University, SE-90871 Umeå, Sweden*

Jyri-Pekka Mikkola − *Wallenberg Wood Science Center, Department of Chemistry Technical Chemistry, Department of Chemistry, Chemical-Biological Centre, Umeå University, SE-90871 Umeå, Sweden; Industrial Chemistry & Reaction Engineering, Johan Gadolin Process Chemistry Centre, Åbo Akademi University, FI-20500 Åbo-Turku, Finland*

Complete contact information is available at:
https://pubs.acs.org/10.1021/acsomega.3c06243

Notes

The authors declare no competing financial interest.

■ REFERENCES

(1) OMS. *Global Action Plan on Antimicrobial Resistance*; World Health Organization, 2017; pp 1−28.

(2) Langford, B. J.; So, M.; Raybardhan, S.; Leung, V.; Soucy, J. P. R.; Westwood, D.; Daneman, N.; MacFadden, D. R. Antibiotic Prescribing in Patients with COVID-19: Rapid Review and Meta-Analysis. *Clin. Microbiol. Infect.* **2021**, *27* (4), 520−531.

(3) dos Santos, A. B.; Cervantes, F. J.; van Lier, J. B. Review Paper on Current Technologies for Decolourisation of Textile Wastewaters: Perspectives for Anaerobic Biotechnology. *Bioresour. Technol.* **2007**, *98* (12), 2369−2385.

(4) Dong, F.; Sun, Y.; Fu, M.; Wu, Z.; Lee, S. C. Room Temperature Synthesis and Highly Enhanced Visible Light Photocatalytic Activity of Porous BiOI/BiOCl Composites Nanoplates Microflowers. *J. Hazard. Mater.* **2012**, *219−220*, 26−34.

(5) Xiao, X.; Hao, R.; Liang, M.; Zuo, X.; Nan, J.; Li, L.; Zhang, W. One-Pot Solvothermal Synthesis of Three-Dimensional (3D) BiOI/BiOCl Composites with Enhanced Visible-Light Photocatalytic Activities for the Degradation of Bisphenol-A. *J. Hazard. Mater.* **2012**, *233−234*, 122−130.

(6) Bao, C.; Wang, H.; Wang, C.; Zhang, X.; Zhao, X.; Dong, C. L.; Huang, Y. C.; Chen, S.; Guo, P.; She, X.; Sun, Y.; Yang, D. Cooperation of Oxygen Vacancy and FeIII/FeII Sites in H2-Reduced

Fe-MIL-101 for Enhanced Fenton-like Degradation of Organic Pollutants. *J. Hazard. Mater.* **2023**, *441* (August2022), 129922.

(7) Han, L.; Zhang, X.; Wu, D. Construction and Characterization of BiOI/NH 2 -MIL-125(Ti) Heterostructures with Excellent Visible-Light Photocatalytic Activity. *J. Mater. Sci.: Mater. Electron.* **2019**, *30* (4), 3773−3781.

(8) Laurier, K. G. M.; Vermoortele, F.; Ameloot, R.; De Vos, D. E.; Hofkens, J.; Roeffaers, M. B. J. Iron(III)-Based Metal-Organic Frameworks as Visible Light Photocatalysts. *J. Am. Chem. Soc.* **2013**, *135* (39), 14488−14491.

(9) Shakly, M.; Saad, L.; Seliem, M. K.; Bonilla-Petriciolet, A.; Shehata, N. New Insights into the Selective Adsorption Mechanism of Cationic and Anionic Dyes Using MIL-101(Fe) Metal-Organic Framework: Modeling and Interpretation of Physicochemical Parameters. *J. Contam. Hydrol.* **2022**, *247* (February), 103977.

(10) Huang, P.; Yao, L.; Chang, Q.; Sha, Y.; Jiang, G.; Zhang, S.; Li, Z. Room-Temperature Preparation of Highly Efficient NH2-MIL-101(Fe) Catalyst: The Important Role of -NH2 in Accelerating Fe(III)/Fe(II) Cycling. *Chemosphere* **2022**, *291* (P3), 133026.

(11) Lee, J.; Kim, K.; Kwon, E. E. Biochar as a Catalyst. *Renewable Sustainable Energy Rev.* **2017**, *77* (February), 70−79.

(12) Vidal, J. L.; Andrea, V. P.; MacQuarrie, S. L.; Kerton, F. M. Oxidized Biochar as a Simple, Renewable Catalyst for the Production of Cyclic Carbonates from Carbon Dioxide and Epoxides. *ChemCatChem* **2019**, *11* (16), 4089−4095.

(13) Ahmaruzzaman, M. Biochar Based Nanocomposites for Photocatalytic Degradation of Emerging Organic Pollutants from Water and Wastewater. *Mater. Res. Bull.* **2021**, *140*, 111262.

(14) Pinna, M.; Binda, G.; Altomare, M.; Marelli, M.; Dossi, C.; Monticelli, D.; Spanu, D.; Recchia, S. Biochar Nanoparticles over Tio2 Nanotube Arrays: A Green Co-Catalyst to Boost the Photocatalytic Degradation of Organic Pollutants. *Catalysts* **2021**, *11* (9), 1048.

(15) Lu, Y.; Cai, Y.; Zhang, S.; Zhuang, L.; Hu, B.; Wang, S.; Chen, J.; Wang, X. Application of Biochar - Based Photocatalysts for Adsorption -(Photo) Degradation/Reduction of Environmental Contaminants: Mechanism, Challenges and Perspective. *Biochar* **2022**, *4*, 45.

(16) Li, X.; Yang, Z.; Wu, G.; Huang, Y.; Zheng, Z.; Garces, H. F.; Yan, K. Fabrication of Ultrathin Lily-like NiCo2O4 Nanosheets via Mooring NiCo Bimetallic Oxide on Waste Biomass-Derived Carbon for Highly Efficient Removal of Phenolic Pollutants. *Chem. Eng. J.* **2022**, *441* (February), 136066.

(17) Huang, Y.; Chen, Y.; Li, X.; Zhu, K.; Jiang, Z.; Yuan, H.; Yan, K. One-Step Solvothermal Construction of Coral Reef-like FeS2/Biochar to Activate Peroxymonosulfate for Efficient Organic Pollutant Removal. *Sep. Purif. Technol.* **2023**, *308* (October2022), 122976.

(18) Subudhi, S.; Tripathy, S. P.; Parida, K. Metal Oxide Integrated Metal Organic Frameworks (MO@MOF): Rational Design, Fabrication Strategy, Characterization and Emerging Photocatalytic Applications. *Inorg. Chem. Front.* **2021**, *8*, 1619−1636.

(19) Chen, Y.; Zhai, B. Y.; Liang, Y. N.; Li, Y. Hybrid Photocatalysts Using Semiconductor/MOF/Graphene Oxide for Superior Photo-degradation of Organic Pollutants under Visible Light. *Mater. Sci. Semicond. Process.* **2020**, *107* (May 2019), 104838.

(20) Fito, J.; Kefeni, K. K.; Nkambule, T. T. I. The Potential of Biochar-Photocatalytic Nanocomposites for Removal of Organic Micropollutants from Wastewater. *Sci. Total Environ.* **2022**, *829*, 154648.

(21) Weidner, E.; Karbassiyazdi, E.; Altaee, A.; Jesionowski, T.; Ciesielczyk, F. Hybrid Metal Oxide/Biochar Materials for Wastewater Treatment Technology: A Review. *ACS Omega* **2022**, *7*, 27062−27078.

(22) Hu, K.; Li, R.; Ye, C.; Wang, A.; Wei, W.; Hu, D.; Qiu, R.; Yan, K. Facile Synthesis of Z-Scheme Composite of TiO2 Nanorod/g-C3N4 Nanosheet Efficient for Photocatalytic Degradation of Ciprofloxacin. *J. Cleaner Prod.* **2020**, *253*, 120055.

(23) Bonilla-Petriciolet, A.; Mendoza-Castillo, D. I.; Elizabeth, R.-Á. H. *Adsorption Processes for Water Treatment and Purification*; Springer International Publishing, 2017.

(24) Salma, A.; Thoröe-Boveleth, S.; Schmidt, T. C.; Tuerk, J. Dependence of Transformation Product Formation on PH during Photolytic and Photocatalytic Degradation of Ciprofloxacin. *J. Hazard. Mater.* **2016**, *313*, 49−59.

(25) Zhu, S.-R.; Liu, P.-F.; Wu, M.-K.; Zhao, W.-N.; Li, G.-C.; Tao, K.; Yi, F.-Y.; Han, L. Enhanced Photocatalytic Performance of BiOBr/NH2-MIL-125(Ti) Composite for Dye Degradation under Visible Light. *Dalton Trans.* **2016**, *45*, 17521−17529.

(26) Almáši, M.; Zeleňák, V.; Palotai, P.; Beňová, E.; Zeleňáková, A. Metal-Organic Framework MIL-101(Fe)-NH2 Functionalized with Different Long-Chain Polyamines as Drug Delivery System. *Inorg. Chem. Commun.* **2018**, *93* (May), 115−120.

(27) Wang, D.; Huang, R.; Liu, W.; Sun, D.; Li, Z. Fe-Based MOFs for Photocatalytic CO2 Reduction: Role of Coordination Unsaturated Sites and Dual Excitation Pathways. *ACS Catal.* **2014**, *4* (12), 4254−4260.

(28) Lu, L.; Kong, C.; Sahajwalla, V.; Harris, D. Char Structural Ordering during Pyrolysis and Combustion and Its Influence on Char Reactivity. *Fuel* **2002**, *81* (9), 1215−1225.

(29) Mansuri, I.; Farzana, R.; Rajarao, R.; Sahajwalla, V. Carbon Dissolution Using Waste Biomass—A Sustainable Approach for Iron-Carbon Alloy Production. *Metals* **2018**, *8* (4), 290.

(30) Qu, S.; Yuan, Y.; Yang, X.; Xu, H.; Mohamed, A. K.; Zhang, J.; Zhao, C.; Liu, L.; Wang, B.; Wang, X.; Rinklebe, J.; Li, Y. C.; Wang, S. Carbon Defects in Biochar Facilitated Nitrogen Doping: The Significant Role of Pyridinic Nitrogen in Peroxymonosulfate Activation and Ciprofloxacin Degradation. *Chem. Eng. J.* **2022**, *441* (February), 135864.

(31) Bu, Y.; Xu, J.; Li, Y.; Liu, Q.; Zhang, X. Enhanced Photocatalytic Activity of BiOI under Visible Light Irradiation by the Modification of MoS2. *RSC Adv.* **2017**, *7* (67), 42398−42406.

(32) Wei, X.; Chen, J.; Xie, Q.; Zhang, S.; Ge, L.; Qiao, X. Distinct Photolytic Mechanisms and Products for Different Dissociation Species of Ciprofloxacin. *Environ. Sci. Technol.* **2013**, *47* (9), 4284−4290.

(33) Paul, T.; Miller, P. L.; Strathmann, T. J. Visible-Light-Mediated TiO2 Photocatalysis of Fluoroquinolone Antibacterial Agents. *Environ. Sci. Technol.* **2007**, *41* (13), 4720−4727.

(34) Salma, A.; Thoröe-Boveleth, S.; Schmidt, T. C.; Tuerk, J. Dependence of Transformation Product Formation on PH during Photolytic and Photocatalytic Degradation of Ciprofloxacin. *J. Hazard. Mater.* **2016**, *313* (0), 49−59.

(35) Hu, X.; Hu, X.; Peng, Q.; Zhou, L.; Tan, X.; Jiang, L.; Tang, C.; Wang, H.; Liu, S.; Wang, Y.; Ning, Z. Mechanisms Underlying the Photocatalytic Degradation Pathway of Ciprofloxacin with Heterogeneous TiO2. *Chem. Eng. J.* **2020**, *380* (July 2019), 122366.

(36) Silva, A. R.; Martins, P. M.; Teixeira, S.; Carabineiro, S. A. C.; Kuehn, K.; Cuniberti, G.; Alves, M. M.; Lanceros-Mendez, S.; Pereira, L. Ciprofloxacin Wastewater Treated by UVA Photocatalysis: Contribution of Irradiated TiO2 and ZnO Nanoparticles on the Final Toxicity as Assessed by Vibrio Fischeri. *RSC Adv.* **2016**, *6* (98), 95494−95503.

(37) Gholizadeh Khasevani, S.; Gholami, M. R. Engineering a Highly Dispersed Core@shell Structure for Efficient Photocatalysis: A Case Study of Ternary Novel BiOI@MIL-88A(Fe)@g-C3N4 Nanocomposite. *Mater. Res. Bull.* **2018**, *106*, 93−102.

(38) Phounglamcheik, A.; Wang, L.; Romar, H.; Kienzl, N.; Broström, M.; Ramser, K.; Skreiberg, Ø.; Umeki, K. Effects of Pyrolysis Conditions and Feedstocks on the Properties and Gasification Reactivity of Charcoal from Woodchips. *Energy Fuels* **2020**, *34* (7), 8353−8365.